Analysis of Nitrogen Fixation by a Catalyst Capable of Transforming N_2, CO_2 and CH_4 into Amino Acids under Mild Reactions Conditions

Guillermo Revilla-López,[1] Jordi Sans,[1,2] Jordi Casanovas,[3] Oscar Bertran,[4] Jordi Puiggalí,[1,2,6,*] Pau Turon[1,5,*] and Carlos Alemán[1,2,6,*]

[1] *Departament d'Enginyeria Química, EEBE, Universitat Politècnica de Catalunya, C/ Eduard Maristany, 10-14, 08019, Barcelona, Spain*

[2] *Barcelona Research Center in Multiscale Science and Engineering, Universitat Politècnica de Catalunya, C/ Eduard Maristany, 10-14, 08019, Barcelona, Spain*

[3] *Departament de Química, EPS, Universitat de Lleida, c/ Jaume II nº 69, Lleida E-25001, Spain*

[4] *Departament de Física EETAC, Universitat Politècnica de Catalunya, c/ Esteve Terrades, 7, 08860, Castelldefels, Spain*

[5] *B. Braun Surgical, S.A. Carretera de Terrasa 121, 08191 Rubí (Barcelona), Spain*

[6] *Institute for Bioengineering of Catalonia (IBEC), The Barcelona Institute of Science and Technology, Baldiri Reixac 10-12, 08028 Barcelona Spain*

[*] jordi.puiggali@upc.edu, pau.turon@bbraun.com and carlos.aleman@upc.edu

ABSTRACT

The processes related to the fixation of nitrogen in a catalyst able to produce glycine and alanine from a N_2, CO_2 and CH_4 gas mixture at mild reaction conditions have been studied by combining experimental and theoretical investigations. Results have allowed to understand the role of different elements of the catalyst, which is constituted by permanently polarized hydroxyapatite (p-HAp), zirconia, and aminotris(methylenephosphonic acid) (ATMP). ATMP attracts N_2 molecules towards the surface, maintaining them close to the zirconia and p-HAp components that are the most active from a catalytic point of view. On the other hand, the associative mechanism is thermodynamically favoured under mild reaction conditions with respect to the dissociative one, which is limited by the barrier associated to the N–N bond cleavage. Because this reaction mechanism is similar to that employed in the nitrogen fixation by nitrogenase enzymes, these findings provide an opportunity to design new bioinspired catalysts.

Keywords: Artificial photosynthesis; Carbon fixation; Hydroxyapatite; N–N bond cleavage

1. Introduction

Nitrogen is an indispensable element of the life and ecosystems on Earth [1]. The main source of nitrogen, dinitrogen (N_2), is the largest single component of Earth atmosphere (~78%). The strong N–N triple bond (226 kcal/mol), the large HOMO-LUMO gap (10.8 eV), and the non-polarity render the N_2 molecule inert towards most reagents [2]. However, the reduction of atmospheric N_2 to ammonia (NH_3), an important precursor for nitrogen-containing compounds, as fertilizers, is one of the most essential processes for nitrogen fixation. In microbiological organisms this process is catalyzed at room temperature and atmospheric pressure by the nitrogenase enzymes [3,4], which operate as follow: a N_2 molecule bonded and activated at the nitrogenase cofactor is protonated and reduced by electrons that stem from a reducing agent.

From an industrial perspective, the production of NH_3 is dominated by the Haber-Bosch process, in which high purity streams of N_2 and H_2 react at high temperatures (~500 ºC) and high pressures (200-300 atm) over iron- or ruthenium-based catalysts [5-7]. Approximately, 20% of the NH_3 synthesized through the Haber-Bosch process, which enables ~50% of the world's food production, is upgraded to nitrogen-containing organic molecules [8]. In addition of its high energetic cost (*i.e.* the Haber-Bosch process accounts 1.4% of world's annual energy consumption) [9], fossil fuels used for heating and pumping the H_2 produce large amount of greenhouse gases. Therefore, it is of great significance to copy natural systems and develop green and sustainable strategies for nitrogen fixation.

The catalytic reduction of N_2 under mild conditions was achieved in early studies using Mo-based catalysts, a mixture of N_2H_4 and NH_3 being obtained [10]. Also, N_2 was converted into NH_3 with excellent yield using protons [11]. Au-surfaces have been used for N_2 reduction, forming N_2H_y species [12]. In a very recent study, Misawa and co-

workers [13] reported a two-electrode plasmon-induced NH_3 synthesis by reducing N_2. This was composed of a strontium titanate photocatalytic anode in which the plasmon effect is expressed by plasmonic gold nanoparticles and a zirconium cathode. However, the nitrogen fixation from N_2 at mild reaction conditions is still considered a very hot topic. For example, Nishibayashi recently developed novel reaction systems for the catalytic transformation of molecular dinitrogen into NH_3 and N_2H_3 using Mo–, Fe–, Co– and V–dinitrogen complexes under mild reaction conditions [14]. In a very recent work [15], we developed an electrophotocatalyst based on hydroxyapatite thermally and electrically stimulated, hereafter denoted permanently polarized hydroxyapatite (p-HAp), and coated with zirconyl chloride (ZC), which supposedly hydrolyzed into zirconia, and aminotris(methylenephosphonic acid) (ATMP) [16]. The new catalyst, p-HAp/ZC/ATMP, allows simultaneously fixation of nitrogen from N_2 and carbon from CO_2 and CH_4 to obtain both glycine and alanine (D/L racemic mixture), the two simplest amino acids, using mild reaction conditions (*i.e.* atmospheric pressure and 95 ºC). With such multi-component catalyst, glycine and alanine molar yields with respect to CH_4 or CO_2 are about 1.9% and 1.6%, respectively, growing up to 3.4% and 2.4% when the gas mixture pressure increases to 6 bars and the reaction temperature is maintained at 95 ºC.

The synthesis of amino acids by direct fixation of nitrogen and carbon from gas mixtures opens new doors for the development of industrial processes based on nitrogen fixation. However, although the general mechanism was hypothesized in our previous study [16], further details about the N_2 cleavage, which is a crucial step for the electrophotosynthesis of glycine and alanine, remained unveiled. Given the importance of understanding the breaking the N–N triple bond on the p-HAp based catalyst, in this

manuscript we report experimental and computational investigations aimed to determine different aspects of this unusual transformation.

2. Methods

2.1. Experiments

p-HAp discs were prepared by applying a constant DC of 500 V at 1000 ºC for 1 hour to previously sintered mineral discs. For this purpose, HAp was synthesized by chemical precipitation, the resulting powder being uniaxially pressed at 620 MPa for 10 min. The resulting discs were sintered by heating at 1000 ºC for 2 hours in air [15].

In order to prepare the p-HAp/ZC/ATMP catalyst, p-HAp discs were sequentially coated with three layers: two layers of ATMP separated by an intermediate layer of ZC [16]. Layers were sequentially applied by depositing some drops of 50 mM ATMP, 10 mM and 50 mM ATMP aqueous solutions. After the deposition of each layer, a drying period of 12 h was applied before drop casting the solution for the next layer.

The hydrolysis of ZC was studied by X-ray photoelectron spectroscopy (XPS), while the ability of p-HAp, zirconia and ATMP to adsorb molecular N_2 was examined by both chemisorption and XPS. For the latter, samples were previously treated in a N_2 atmosphere at 95 ºC for 1, 2, 4, and 6 bars of pressure. The pressure in the analysis chamber was always below 10^{-7} Pa before XPS measurements. Detailed description of the adsorption experiments, which were performed at 95 ºC as the catalytic synthesis of amino acids [16], is provided in the ESI.

NMR 2D ^{1}H–^{15}N Heteronuclear Single-Quantum Correlation (HSQC) assays were performed using a Brucker Avance DRX-500-CRYO equipped with a TCl (5 mm) cryo-probe operating at 500 MHz and 50 MHz per for ^{1}H and ^{15}N, respectively. A total of 700 scans were recorded. ^{1}H and ^{13}C NMR spectra in solution were obtained after

extraction of the amino acids from the catalyst by dissolving the sample in deuterated water containing 100 mM of HCl and 50 mM of NaCl at 25 ºC. ^{1}H NMR spectra were acquired with a Bruker Ascend 400 spectrometer operating at 400 MHz. Chemical shifts of all liquid state NMR spectra (^{1}H and ^{13}C) were calibrated using tetramethylsilane as an internal standard.

Thermal degradation of ATMP samples was studied at a heating rate of 20 ºC/min (sample weight *ca.* 5 mg) with a Q50 thermogravimetric analyzer of TA Instruments and under a flow of dry nitrogen. Test temperatures ranged from 30 to 545 ºC.

2.2. Molecular Dynamics (MD) simulations

The adsorption of N_2 molecules onto p-HAp, zirconia, and ATMP layers was examined using atomistic MD simulations, which were conducted considering the (0001) facet of the hexagonal HAp unit cell ($a = b$ = 9.421 Å, c = 6.881 Å, $\alpha = \beta = 90°$, and $\gamma = 120°$), the (101) facet of the monoclinic zirconia (a = 5.17 Å, b =5.23 Å, c = 5.3 Å, $\alpha = \gamma = 90°$, and $\beta = 99.25º$) and an amorphous layer of ATMP. In order to capture the physics of the system by applying periodic boundary conditions, the size of the simulated model (*i.e.* number of p-HAp and ZC cells and number of ATMP and N_2 molecules) was selected be large enough to prevent periodic artifacts from occurring due to the unphysical topology of the simulation (i.e. to prevent interactions with its own image in a neighboring simulation box). The model for the p-HAp consisted on a 20 × 20 supercell reconstruction with a mineral thickness in the z direction corresponding to 10 unit cells (*i.e.* >20 Å). The ZC model was built considering a 10 × 9 supercell with ~3.5 layers. Finally, amorphous ATMP was modeled using 256 molecules distributed in a 53.8 × 54.3 Å^2 amorphous surface with a thickness of ~20 Å. A total of 256 N_2 molecules were introduced in the simulation box of each system.

Production MD trajectories (1 μs for each system) were run with the NAMD software package [17] using the Amber force-field [18]. Details about the force-field parameters, the constructed systems and the simulation conditions are provided in the Supporting Information.

2.3. Density Functional Theory (DFT) calculations

DFT calculations were performed using the PBE1PBE hybrid functional [19,20] combined with the LANL2DZ basis set [21-24] within the spin unrestricted formalism (*i.e.* the spin multiplicity rendering the lowest energy system was used in each case). The PBE1PBE combines the so called PBE generalized gradient functional with a predefined amount of exact exchange, providing a satisfactory description of structural, kinetic, spectroscopic and electronic properties [19]. The performance of this functional to study the N_2 adsorption and activation on inorganic surfaces was previously demonstrated [25]. Besides, LANL2DZ basis set was specifically designed to model metal-containing systems, as is the case for HAp and ZrO_2 [21-24].

All structures were submitted to complete geometry optimizations and frequency calculations, the latter being determined under the harmonic approximation used by the software. All the minima exhibited real frequencies while transition states were characterized by one imaginary frequency. Thermochemical analysis based on harmonic vibrational frequencies was used to derive the free energies for all species calculated in the analysed mechanisms. All calculations were conducted using the Gaussian 09 software suite [26].

The interaction between N_2 and the mineral surfaces was simulated through clusters, which were built to represent the (0001) and the (101) facet of HAp and ZrO_2, respectively. The coordinates of the mineral cluster were kept frozen through all

calculations, thus only allowing the atoms of nitrogen molecules and its derivatives to freely move. The cluster systems represented the non-periodic supercells $1 \times 2 \times 2$ and $2 \times 1 \times 1$ for ZrO_2 and HAp respectively, thus encompassing a system composition of $Zr_{16}O_{32}$ and $Ca_{20}(PO_4)_{12}(OH)_3$.

3. Results and discussion

3.1. Hydrolysis of zirconyl chloride into zirconia

In our previous work, the ZC ($ZrOCl_2 \cdot 8H_2O$) coating was assumed to hydrolyze into zirconia since the environment employed for the catalytic transformation of N_2, CO_2 and CH_4 into amino acids is suitable to force, at least partially, the hydrolysis [16]. This hypothesis, which is crucial for the modeling of the photo-active surface, has been corroborated in the present work by comparing a layer of ZC as prepared and after treatment for 1 hour at 95 ºC in a water vapor atmosphere. The latter conditions mimic those used for the production of amino acids using the p-HAp/ZC/ATMP catalyst [16]. Comparison of the atomic compositions, as determined by XPS (Table 1), reflects a drastic reduction in the chlorine concentration, demonstrating that ZC hydrolyzed into zirconia predominates under the reaction conditions. Therefore, in next sections the monoclinic cell of zirconia was used to model not only the adsorption of N_2 molecules but also the N–N cleavage mechanism.

3.2. N_2 adsorption

The radial distribution functions of Surf$\cdots N_2$ atom pairs, $g_{Surf\text{-}N2}(r)$, which refer to the distance between any atom of p-HAp, zirconia or ATMP surface and a nitrogen atom of the N_2 molecule, obtained from MD simulations are displayed in Figure 1a. As it can be seen, the shape of the profiles involving charged p-HAp and zirconia surfaces

is completely different from that of ATMP. More specifically, linear profiles with similar slopes were obtained for p-HAp and zirconia, evidencing that N_2 molecules exhibit a Brownian motion with no preferential position or direction of flow. Thus, the tendency of such charged surfaces to adsorb non-polar N_2 molecules is null. The shape of the $g_{Surf\text{-}N2}(r)$ profile changes completely for ATMP, exhibiting two peaks of similar intensities centred at 4.05 and 5.75 Å, which correspond to the adsorbed N_2 molecules. Furthermore, the height of the profile at the r < 9 Å evidences the very remarkable affinity between the ATMP surface and the gaseous N_2 molecules. At increasing r values the profile follows a decreasing tendency, which is opposite to that observed for p-HAp and zirconia, and shows the accumulation of gas molecules at regions close to the ATMP surface.

The attractive interactions between the ATMP surface and the N_2 molecules have been monitored by examining the radial distribution functions for ATMP(#)···N_2 atom pairs, $g_{ATMP(\#)\text{-}N2}(r)$ (where # refers to the C, O, P and N atoms of ATMP; and N_2 to each nitrogen atom of N_2), and are displayed in Figure 1b. As it can be seen, N_2 molecules tend to be predominantly adsorbed close to the oxygen atoms of ATMP, the $g_{ATMP(O)\text{-}N2}(r)$ profile showing two intense peaks at 3.55 and 5.75 Å. Besides, the curves obtained for the C and N atoms of ATMP display two (4.15 and 5.85 Å) peaks and one (4.85 Å) peak, respectively, even though these are much intense than those obtained for $g_{ATMP(O)\text{-}N2}(r)$. Finally, the weak peak of $g_{ATMP(N)\text{-}N2}(r)$ at 4.95 Å evidences that the adsorption of N_2 close to the N atoms of ATMP is not particularly favored. According to these results, the physical adsorption of N_2 onto the ATMP surface has been associated to attractive O···N and H···N van der Waals interactions, the latter being responsible of the shift detected in the first peak of $g_{ATMP(O)\text{-}N2}(r)$ at 3.55 Å to 4.05 Å as observed in $g_{Surf\text{-}N2}(r)$ for ATMP (Figure 1a). Figure 1c displays a representative snapshot of the

simulation conducted for ATMP, details of the O···N and H···N van der Waals interactions (*i.e.* the two atoms are separated by less than 4 Å) being also provided for a representative adsorbed N_2 molecule (inset).

Analysis of the trajectory reflects that the adsorption of N_2 molecules is a very frequent event, even though they reside for very short lapse of time on the adsorbent ATMP surface. Figure 1d represents the distribution of the maximum time (t_{max}) in which the N_2 molecules remain uninterruptedly at a distance smaller than 4 Å from any atom of the surface for the 1 μs trajectory. As it can be seen, the profile exhibits a bimodal Gaussian-like shape with an intense peak at ~7 ns and a weak peak at 14 ns. A few N_2 molecules exhibit t_{max} values comprised between 20 and 27 ns. These short values indicate that N_2···ATMP interactions are extremely labile and, therefore, experimental measures of the equilibrium sorption are challenging (see below). Indeed, the kinetics of the adsorption and desorption processes are extremely fast, as it is evidenced in Figure 1e that represents the distribution of accumulated time (t_{acc}) for the N_2 molecules that remain at a distance smaller than 4 Å from any atom of the surface during the 1 μs trajectory. The values of t_{acc} range from 145 to 196 ns, the maximum being located at 168 ns. Considering the average values of t_{max} and t_{acc} (8 and 173 ns, respectively), it is estimated that each gas molecule experiences ~22 adsorption-desorption processes in average.

Exceptions to this behaviour are the three molecules marked with red arrows in the inset of Figure 1d, which exhibit t_{max} values of 249, 334 and 988 ns. It is worth noting that these N_2 molecules do not adsorb onto the ATMP surface but solubilize into the matrix. This is reflected in Figure 1f, which shows a selected snapshot with the three solubilized N_2 molecules completely embedded into the organic layer.

Programmed measurements of N_2 desorption experiments were unfeasible due to the weak strength of the interaction forces between the gas molecules and the ATMP surface, which were extremely weak as showed by MD simulations. Thus, Figure S1 evidences that, after several pulses, the programmed desorption curve is almost identical to the initial ones.

Accordingly, the N_2 adsorption ability of p-HAp, ZC partially hydrolyzed into zirconia and ATMP was examined by XPS. For this purpose, a gas line connected to a chamber was used to introduce N_2 at pressure of 1, 2, 4, or 6 bars during 1 h. Along the process, the temperature was kept at 95 ºC, which was the one used for the synthesis of amino acids by direct fixation of nitrogen [16]. After that period of time, the sample was transferred to the analysis chamber for measurements at a pressure below 10^{-7} Pa. Comparison of the atomic percent composition of the samples before and after apply the gas flux indicates that ATMP is the only compound able to adsorb a significant amount of N_2 (Figures 2 and S2), which is in excellent agreement with MD predictions.

Figures 2a, 2b and 2c display high-resolution XPS spectrum in the N1s region for ATMP samples as prepared, after 1 h in a N_2 atmosphere at 1 bar, and after 1 h in a N_2 atmosphere at 6 bars, respectively. As is shown, deconvolution led to three components in all cases. The two most intense at 400 and 402 eV are attributable to the $^{+}N(CH_2)^{3-}$ and $N(CH_2)^{3-}$ of ATMP, while the third at 405 eV has been ascribed to molecular N_2 triple bond. Analysis of the variation of the weight percent contribution of each component with the pressure of N_2 during the adsorption treatment indicates that adsorption of N_2 remains around 2% (*i.e.* from 1.6 to 2.1%), even after the pressure of the chamber was reduced 10^{-7} Pa for analysis (see Methods section). It should be noted that the difference between these XPS experiments and the programmed measurements of N_2 desorption is that, in the former, the vacuum was applied progressively. The

gradual elimination of the gas facilitated the adsorption of N_2 molecules, even though they interact very weakly with the substrate. Therefore, such ~2% should be considered as the intrinsic N_2 adsorption capacity of ATMP. Indeed, the weight of the N_2 component for pristine ATMP is 1.7%. This observation is consistent with the fact that the molar yields of amino acids in the reaction catalyzed by p-HAp/ZC/ATMP increased moderately when the N_2 partial pressure in the reaction grew from of 0.33 to 2 bar (*i.e.* from 3.5% to 5.8%) [16]. On the other hand, the detection of the nitrogen peak in the spectra recorded for p-HAp and partially hydrolyzed ZC after 1 h in a N_2 atmosphere at 6 bars was null.

Overall, MD and XPS results indicate that the ATMP layer of the p-HAp/ZC/ATMP catalyst acts as a N_2 reservoir. Considering that ATMP is a relatively inert compound and is not expected to participate actively in the nitrogen fixation process, its properties are suitable to play a passive but key role, attracting N_2 molecules towards the surface of the active elements of the catalyst. This is consistent with the covering power of the ATMP, as observed by SEM (Figure 3a), which forms micrometric islands that partially coats the surface of the catalyst. Indeed, previous results evidenced that the nitrogen fixation reaction is not possible in absence of ATMP [16].

3.3. Experimental assessment of N_2 fixation

The p-HAp/ZC/ATMP catalyst was prepared as is described in the Methods section. The SEM micrograph displayed in Figure 3a, which shows the distribution of the three components, indicates that ZC and ATMP aggregates are disseminated onto the surface of p-HAp. ATMP aggregates present two different morphologies: laminated plates and 3D flower-shape structures, while ZC tends to organize in clusters of small globular corpuscles. Then, the N_2 fixation has been experimentally studied analysing both the

amino acids produced using the p-HAp/ZC/ATMP catalyst and the possible degradation products of the ATMP coating after such reaction.

The synthesis of glycine and alanine was carried out in an inert reaction chamber, which is described in the ESI, with a weakly reducing atmosphere constituted by CO_2 (2 bar), CH_4 (2 bar), N_2 (2 bar: 1 bar $^{14}N_2$ + 1 bar $^{15}N_2$) and liquid H_2O, using an UV lamp (λ= 254 nm) directly irradiating the catalyst and gas mixture, as was already described [16]. The success of the reaction was confirmed after 48 h by acquiring the ^{1}H and ^{13}C the NMR spectra of the samples obtained by dissolving the catalyst and products of reaction (Figure S3), results being fully consistent with those reported in our recent study [16]. As shown in the 2D $^{1}H–^{15}N$ HSQC NMR spectrum displayed in Figure 3b, in addition of the artifact lines from the water solvent, $^{1}H–^{15}N$ HSQC signal intensities appear near the top of the spectrum. Peaks at such region are attributable to the NH_2 backbone of glycine and alanine, which are known to be sensible to the environment [27,28]. In spite of this, 2D $^{1}H–^{15}N$ HSQC should be considered as ambiguous due to the weakness of the signal intensities, which has been attributed to the low yield of the reaction (*i.e.* 0.6% and 2.1% for glycine and alanine, respectively).

In order to complement 2D $^{1}H–^{15}N$ HSQC results, additional studies have been conducted to check the possible existence of degradation products coming from ATMP, which might another source of nitrogen be discarded. Figure 3c shows the curves derived from the thermal gravimetric analyses (TGA) and the differential thermogravimetric analyses (DTGA) for ATMP as purchased and after being treated with UV radiation at 95 ºC for 48 h, the latter conditions being identical to those used in the catalytic reaction of amino acids. TGA results reflect that the UV radiation and the temperature do not influence the thermal stability of ATMP. Both samples are stable up to a temperature of ~170 ºC, which is much higher than that used for the reaction. Thus,

the temperatures at a 5% weight loss ($T_{5\%}$) are around 255 and 246 ºC for purchased and treated ATMP, respectively. DGTA curves show the first pronounced degradation step at around 220 ºC, even though above such temperature the degradation of the two samples follows different mechanisms.

In a recent study the products and intermediates from decomposition of aminopolyphosphonates, including ATMP, were proposed to be aminomethylphosphonic acid (AMPA), 2-aminethylphosphonic acid (2-AEP), methylamine, *N*-phosphonomethyl-glycine (NMPG) and *N*-(methyl)glycine (SAR) [29]. Figure 4 compares the ^{1}H NMR spectrum of a sample obtained by dissolving the catalyst and products of reaction with the spectra of the proposed decomposition products and intermediates dissolved in the same medium (*i.e.* deuterated water containing 100 mM of HCl and 50 mM of NaCl at 25 ºC). As is shown, the former displays the ATMP methylene group (doublet at 3.52-3.56 ppm) and the signals corresponding to produced amino acids, such as methylene protons (singlet at 3.36 ppm) of glycine and both methine (quadruplet at 3.82-3.86 ppm) and methyl (doublet at 1.60-1.622 ppm) groups of Ala. These signals do no overlap with those recorded for the proposed ATMP decomposition products (Figure 4). Overall, although 2D ^{1}H–^{15}N HSQC NMR analyses were not conclusive enough to unambiguously prove the formation of ^{15}N labelled glycine and alanine, ^{1}H NMR analyses of the AMTP decomposition products and intermediates support the N_2 fixation.

Finally, in order to ascertain the importance of the photon in the production of amino acids, the synthesis of glycine and alanine was attempted without UV radiation but increasing progressively the temperature from 95 ºC to 120 ºC. The reaction was unsuccessful in all cases, suggesting that photoirradiation is important for the nitrogen fixation, which is in agreement with recent observations [16].

3.4. Mechanism for N–N triple bond cleavage

Quantum mechanical calculations have been revealed to be very useful for investigating catalytic reaction mechanisms [30,31]. The amino acids formation requires a complex mechanism with many reaction steps that cannot be afforded without complete understanding of the simplest steps. Among them, the most intriguing is the N_2 fixation due to the N–N triple bond cleavage. In this section, DFT calculations have been used to asses details of various mechanisms for the N–N triple bond cleavage on the p-HAp/ZC/ATMP catalyst. For this purpose, both the associative and dissociative mechanisms (hereafter, AM and DM, respectively), which are the two most accepted mechanisms for N_2 fixation, have been investigated. In the AM, N_2 molecules are protonated sequentially without breaking the N–N bond until producing the first amine molecule. This reaction mechanism, which is motivated by that observed in Nature for nitrogenases enzymes [4], has been recently proposed for some bioinspired catalysts that transform N_2 into NH_3 by photochemical reduction [32-35]. In the DM, N_2 molecules dissociate at the beginning of the reaction and each resulting radical evolves towards an amine, as occurs in the Haber-Bosch process using Ru- and Fe-metal based catalyst [36-41]. Furthermore, the pathway for each mechanism has been examined considering both p-HAp and zirconia surfaces, which have been represented using $[Ca_{20}(PO_4)_{12}(OH)_3]^{+1}$ and $Zr_{16}O_{32}$ clusters, respectively. According to its inert chemical nature, the role attributed to the ATMP is to attract N_2 molecules, acting as a reservoir for subsequent reaction on the catalytic surface, as is consistent with results displayed in the previous section.

The reaction pathways for the AM and DM are schematically depicted in Figures 5a and 6a, respectively. For simplicity, the R^+ specie, which should be CH_3^+ from CH_4 in

the experimental setup, was replaced by H^+ in theoretical calculations. This simplification not only retains the most relevant chemical features of the studied mechanisms but also allows obviating the order of the steps related with the incorporation of H^+ from water and of CH_3^+ from CH_4, which is not a relevant goal for this study. On the other hand, although several of the reaction steps depicted in Figures 5 and 6 are expected to involve an activation barrier, the calculation of the transition states has been restricted for the first steps of each pathway only, which will determine the preference towards the AM or the DM.

The AM consists of five steps according to which the N_2 from the reactor atmosphere (A) is adsorbed onto the substrate (B). After this, it reacts with protons coming from water through the substrate to yield $N–NH^+$ (C) and, subsequently, $(N–NH_2)^+$ (D) that dissociates into released NH_2R (*i.e.* NH_3 in the model reaction) and adsorbed N^{3+} (E). Figure 5b represents the diagrams with the free energies of the reaction intermediates for the AM once the N_2 has been activated by binding onto the p-HAp and zirconia. It is worth mentioning that no activation barrier was detected in this mechanism for the protonation of the adsorbed N_2 molecule (B→C).

When the associative reaction occurs onto the zirconia surface (hereafter AM/ZN) the N_2 binds to the zirconium cation, while the N_2 adsorbs onto an oxygen atom from the phosphate when the reaction takes place onto the p-HAp (hereafter AM/p-HAp). The former process results in an energy gain of 1.07 eV with respect to the latter. This limits the AM/p-HAp process with respect to the AM/ZN, which is also the most favored process for the rest of steps in the reaction pathway. This result clearly indicates that the AM/ZN is the most probable mechanism if N_2 molecules are protonated without breaking the N–N bond.

In the DM, the N–N bond dissociates at the very beginning of the reaction, before the adsorption onto the substrate. This initial dissociation is expected to require a high kinetic barrier, suggesting that it is the limiting step of the reaction. Once the N_2 molecule dissociates, each nitrogen radical is protonated to produce NH_2R analogously to the Haber-Bosch process [36]. In the reaction pathway studied for the DM, which is depicted in Figure 6a, the R^+ specie was replaced by H^+ in the calculations by analogy with the AM. Besides, when the N–N bond dissociation occurs near the p-HAp or zirconia substrate for subsequent adsorption of the resulting nitrogen radical, the resulting mechanisms have been denoted DM/p-HAp and DM/ZN.

The DM mechanism is limited with respect to the AM by the activation barrier associated to the N–N cleavage in the A→B step (Figure 6b). In order to evaluate this barrier, the transition state (TS) was calculated for both DM/p-HAp and DM/ZN. The N–N bond elongates by about 33% as compared to the equilibrium value (1.12 Å) and the barrier is very high (> 40 kcal/mol) in both cases, reflecting that the DM mechanism is much less probable than the AM under mild conditions. Besides, the activation energy is 2.7 kcal/mol higher for DM/p-HAp than for DM/ZN.

The adsorption of the dissociated nitrogen atoms occurs onto oxygen atoms, even though this process is more favored for DM/ZN than for DM/p-HAp. Moreover, the free energy for the A→B step is disfavored by 7.8 eV for the DM/p-HAp while it is favored by 6.6 eV for the DM/ZN. Although the rest of steps are energetically favored for the two dissociative reaction pathways, both the activation barrier and the reaction energy of the A→B step favours the DM/ZN with respect to the DM/p-HAp.

Other pathways, as for example the one proposed by Solans-Monfort *et al.* [42] for N_2 cleavage by H_2 in the presence of silica-supported tantalum hydride complexes, have been analysed. In all cases the calculated barrier was significantly higher than those

obtained not only for the AM but also for the DM. In particular, Zr–N_2–Zr reactive complexes were not stable enough to be considered as an alternative to the reactive AM and DM pathways.

In summary, comparison between the DFT results displayed in Figures 5 and 6 indicates that nitrogen fixation through the DM is less probable than through the AM under mild conditions, like those used for yielding glycine and alanine. In order to overcome the high activation barrier connected with transition state of the A→B step in the DM, harsh temperature and pressure conditions would be required. In contrast, the AM predicts that the formation of reactive Zr–N_2 and subsequent nitrogen hydrogenation, N–N cleave, and release of the corresponding amines is thermodynamically favored. It is worth noting that the AM was also proposed for the NH_3 photosynthesis using a plasmonic photoanode and a zirconium cathode for N_2 reduction [13].

4. Conclusions

Investigations into the mechanism of p-HAp/ZC/ATMP induced N_2 cleavage under mild conditions to from amino acids in presence of CO_2 and CH_4 have been carried out. The nitrogen fixation has been studied using isotopic labeled $^{15}N_2$ in the feeding mixture and, subsequently, monitoring the formation of ^{15}N labeled glycine and alanine by 2D ^{1}H–^{15}N HSQC NMR. Computational studies based on classical force-field MD simulations and DFT calculations have been used to determine the role of the different components of the catalyst in the nitrogen fixation process. MD results indicate that ATMP weakly attracts the N_2 molecules towards the surface of the catalysts, whereas p-HAp and zirconia are not able to exert such effect. This computational prediction has been corroborated experimentally by XPS experiments. Besides, DFT calculations

indicate that the N–N cleavage occurs onto the zirconia surface, after the formation of $Zr–N_2$ complexes, following an associative mechanism similar to that observed in Nature for nitrogenase enzymes. These results suggest that p-HAp is mainly involved in the fixation of carbon from CO_2 and/or CH_4, or even in the coupling of the different radicals to produce the final assembly of amino acids. Although we are currently conducting further refinements to ascertain such important point that would allow to complete this complex catalytic process as a whole, we consider that the new findings described in this paper provide a new opportunity to design and develop more effective nitrogen fixation under mild reaction conditions.

Acknowledgements

This work was supported by MINECO-FEDER (RTI2018-098951-B-I00 and RTI2018-101827-B-I00), by B. Braun Surgical S.A. through a joint research agreement with UPC, and by the Agència de Gestió d'Ajuts Universitaris i de Recerca (2017SGR359 and 2017SGR373). This work is integrated within a wider research project supported by B. Braun Surgical S.A., UPC, ICS and ICFO. Support for the research of C.A. was received through the prize "ICREA Academia" for excellence in research funded by the Generalitat de Catalunya.

Declaration of interest

Authors declare that the preparation and application of permanently polarized hydroxyapatite was patented by the Universitat Politcnica de Catalunya and B Braun Surgical S.A. (EP16382381, EP16382524, P27990EP00, PCT/EP2017/069437).

References

[1] D. E. Canfield, A. N. Glazer, P. G. Falkowski, Science 330 (2010) 192–196. https://doi.org/10.1126/science.1186120

[2] H.-P. Jia, E. A. Quadrelli, Chem. Soc. Rev. 43 (2014) 547–564. https://doi.org/10.1039/C3CS60206K

[3] Y. Hu, M. W. Ribbe, Methods Mol. Biol. 766 (2011) 3–7. https://doi.org/10.1007/978-1-61779-194-9_1

[4] B. M. Hoffman, D. Lukoyanov, D. R. Dean, L. C. Seefeldt, Acc. Chem. Res. 46 (2013) 587–595. https://doi.org/10.1021/ar300267m

[5] S. F. Foster, S. I. Perez-Bakovic, R. D. Duda, S. Maheshwari, R. D. Milton, S. D. Minteer, M. J. Janik, J. N. Renner, L. F. Greenless, Nat. Catal. 1 (2018) 490–500. https://doi.org/10.1038/s41929-018-0092-7

[6] K. Aika, A. Ohya, A. Ozaki, Y. Inoue, I. Yasumori, J. Catal. 92 (1985) 305–311. https://doi.org/10.1016/0021-9517(85)90265-9

[7] J. Fajardo, J. C. Peters, J. Am. Chem. Soc. 139 (2017) 16105–16108. https://doi.org/10.1021/jacs.7b10204

[8] T. Oshikiri, K. Ueno, H. Misawa, Angew. Chem. Int. Ed. 55 (2016) 3942–3946. https://doi.org/10.1002/anie.201511189

[9] C. J. M. van der Ham, M. T. M. Koper, D. G. H. Hetterscheid, Chem. Soc. Rev. 43 (2014) 5183–5191. https://doi.org/10.1039/C4CS00085D

[10] A. E. Shilov, Russ. Chem. Bull. Int. Ed. 52 (2003) 2555. https://doi.org/10.1023/B:RUCB.0000019873.81002.60

[11] D. V. Yandulov, R. R. Schrock, Science 301 (2003) 76–78. https://doi.org/10.1126/science.1085326

[12] Y. Yao, S. Zhu, H. Wang, H. Li, M. Shao, J. Am. Chem. Soc.140 (2018) 1496. https://doi.org/10.1021/jacs.7b12101

[13] T. Oshikiri, K. Ueno, H. Misawa, Green Chem. 21 (2019) 4443. https://doi.org/10.1039/C9GC01658A

[14] Y. Nishibayashi, Dalton Trans. 47 (2018) 11290–11297. https://doi.org/10.1039/C8DT02572J

[15] M. Rivas, L. J. del Valle, E. Armelin, O. Bertran, P. Turon, J. Puiggalí, C. Alemán, Chem. Phys. Chem. 19 (2018) 1746–1755. https://doi.org/10.1002/cphc.201800196

[16] M. Rivas, L. J. del Valle, P. Turon, C. Alemán, J. Puiggalí, Green Chem. 20 (2018) 685–693. https://doi.org/10.1039/C7GC02911J

[17] J. C. Phillips, R. Braun, W. Wang, J. Gumbart, E. Tajkhorshid, E. Villa, C. Chipot, R. D. Skeel, L. Kale, K. Schulten, J. Comput. Chem. 26 (2005) 1781–1802. https://doi.org/10.1002/jcc.20289

[18] W. D. Cornell, P. Cieplak, C. I. Bayly, I. R. Gould, K. M. Merz, D. M. Ferguson, D. C. Spellmeyer, T. Fox, J. W. Caldwell, P. A. Kollman, J. Am. Chem. Soc. 117 (1995) 5179–5197. https://doi.org/10.1021/ja00124a002

[19] C. Adamo, V. Barone, J. Chem. Phys. 110 (1998) 6158–6170. https://doi.org/10.1063/1.478522

[20] M. Ernzerhof, J. P. Perdew, J. Chem. Phys. 109 (1998) 3313–3320. https://doi.org/10.1063/1.476928

[21] T. H. Dunning Jr., P. J. Hay, in Modern Theoretical Chemistry, Ed. H. F. Schaefer III, Vol. 3, Plenum, New York, 1977, pp 1–28.

[22] J. Hay, W. R. Wadt, J. Chem. Phys. 82 (1985) 270–283. https://doi.org/10.1063/1.448799

[23] W. R. Wadt, P. J. Hay, J. Chem. Phys. 82 (1985) 284–298. https://doi.org/10.1063/1.448800

[24] P. J. Hay, W. R. Wadt, J. Chem. Phys. 82 (1985) 299–310. https://doi.org/10.1063/1.448975

[25] C. D. Zeinalipour-Yazdi, J. S. J. Hargreaves, C. R. A. Catlow, J. Phys. Chem. C 119 (2015) 28368–28376. https://doi.org/10.1021/acs.jpcc.5b06811

[26] Gaussian 09, Revision A.02, M. J. Frisch, G. W. Trucks, H. B. Schlegel, G. E. Scuseria, M. A. Robb, J. R. Cheeseman, G. Scalmani, V. Barone, B. Mennucci, G. A. Petersson, H. Nakatsuji, M. Caricato, X. Li, H. P. Hratchian, A. F. Izmaylov, J. Bloino, G. Zheng, J. L. Sonnenberg, M. Hada, M. Ehara, K. Toyota, R. Fukuda, J. Hasegawa, M. Ishida, T. Nakajima, Y. Honda, O. Kitao, H. Nakai, T. Vreven, J. A. Montgomery Jr, J. E. Peralta, F. Ogliaro, M. Bearpark, J. J. Heyd, E. Brothers, K. N. Kudin, V. N. Staroverov, R. Kobayashi, J. Normand, K. Raghavachari, A. Rendell, J. C. Burant, S. S. Iyengar, J. Tomasi, M. Cossi, N. Rega, J. M. Millam, M. Klene, J. E. Knox, J. B. Cross, V. Bakken, C. Adamo, J. Jaramillo, R. Gomperts, R. E. Stratmann, O. Yazyev, A. J. Austin, R. Cammi, C. Pomelli, J. W. Ochterski, R. L. Martin, K. Morokuma, V. G. Zakrzewski, G. A. Voth, P. Salvador, J. J. Dannenberg, S. Dapprich, A. D. Daniels, O. Farkas, J. B. Foresman, J. V. Ortiz, J. Cioslowski, D. J. Fox, Gaussian, Inc., Wallingford, CT, 2009.

[27] K. K. Singarapu, M. Tonelli, D. C. Chow, R. O. Frederick, W. M. Westler, J. Markley, J. Biol. Chem. 286 (2011) 43447–43453. https://doi.org/10.1074/jbc.M111.306464

[28] C. Guo, J. S. Jordan, J. L. Yarger, G. P. Holland, ACS Appl. Mater. Interfaces 9 (2017) 17653−17661. https://doi.org/10.1021/acsami.7b04887

[29] D. Drzyzgai, J. Lipok, Environ. Sci. Pollut. Res., 2017, 24, 24364−17661. https://doi.org/10.1007/s11356-017-0068-1

[30] D. Zheng, P. Ning, J. Jiang, F. Liu, L. Wang, J. Zhang, J. Mol. Liq., 2019, 284, 68−74. https://doi.org/10.1016/j.molliq.2019.03.165

[31] D. Zheng, J. Zhang, X. Zhu, R. Ren, L. Wang and J. Zhang, J. CO2 Util., 2018, 27, 99−106. https://doi.org/10.1016/j.jcou.2018.07.005

[32] J. R. Fryer, J. L. Hutchison, R. Paterson, J. Colloid Interface Sci. 34 (1970) 238–248. https://doi.org/10.1016/0021-9797(70)90175-X

[33] B. M. Hoffman, D. R. Dean, L. C. Seefeldt, Acc. Chem. Res. 42 (2009) 609–619. https://doi.org/10.1021/ar8002128

[34] J. Liu, M. S. Kelley, W. Q. Wu, A. Banerjee, A. P. Douvalis, J. S. Wu, Y. B. Zhang, G. C. Schatz, M. G. Kanatzidis, Proc. Natl. Acad. Sci. USA 113 (2016) 5530–5535. https://doi.org/10.1073/pnas.1605512113

[35] C. Liu, K. K. Sakimoto, B. C. Colon, P. A. Silver, D. G. Nocera, Proc. Natl. Acad. Sci. USA 114 (2017) 6450–6455. https://doi.org/10.1073/pnas.1706371114

[36] J. C. Liu, X. L. Ma, Y. Li, Y. G. Wang, H. Xiao, J. Li, Natur. Commun. 9 (2018) 1610. https://doi.org/10.1038/s41467-018-03795-8

[37] M. Falcone, L. Chatelain, R. Scopelliti, I. Zivkovic, M. Mazzanti, Nature 547 (2017) 332–335. https://doi.org/10.1038/nature23279

[38] T. H. Rod, A. Logadottir, J. K. Nørskov, J. Chem. Phys. 112 (2000) 5343–5347. https://doi.org/10.1063/1.481103

[39] A. Logadóttir, J. K. Nørskov, J. Catal. 220 (2003) 273–279. https://doi.org/10.1016/S0021-9517(03)00156-8

[40] S. F. McWilliams, P. L. Holland, Acc. Chem. Res. 48 (2015) 2059–2065. https://doi.org/10.1021/acs.accounts.5b00213

[41] T. Kandemir, M. E. Schuster, A. Sehyshyn, M. Behrens, R. Schlogl, Angew. Chem. Int. Ed. 52 (2013) 12723–12726. https://doi.org/10.1002/anie.201305812

[42] X. Solans-Monfort, C. Chow, E. Goure, Y. Kaya, J.-M. Basset, M. Taoufik, E. A. Quadrelli, O. Eisenstein, Inorg. Chem. 51 (2012) 7237–7249. https://doi.org/10.1021/ic300498b

Table 1. Atomic percent composition (Zr, O and Cl) obtained by XPS for zirconyl chloride coatings as prepared and after 1 hour at 95 ºC in water vapor atmosphere.

	Zr	**O**	**Cl**
zirconyl chloride coating, as prepared	18.23	45.98	35.78
zirconyl chloride coating after 1 h treatment	28.91	56.00	15.08

CAPTIONS TO FIGURES

Figure 1. (a) Radial distribution functions for the pairs of atoms involving one of the tested surfaces (any atom from HAp, ATMP or ZC) and the nitrogen from N_2. (b) Radial distribution functions for the pairs involving the C, O, P or N atoms of ATMP and a nitrogen atom from N_2. (c) Representative snapshot showing the adsorption of N_2 molecules (light blue: $t_{max} < 7$ ns; intense blue:7 ns $\leq t_{max}$ 10 ns; light red: 10 ns $\leq t_{max}$ 13 ns; and red: $t_{max} \geq 14$ ns) onto the the ATMP layer (in grey). The inset represents details about the van der Waals interactions involved in the adsorption of one representative N_2 molecule. All ATMP atoms at a distance lower than 4 Å from any of the two nitrogen atoms of N_2 are coloured: Oxygen and hydrogen atoms in red and white, respectively. (d) For the 1 μs trajectory, maximum time (t_{max}) distribution of N_2 molecules that remain uninterrupted at a distance smaller than 4 Å from any atom of the surface. The inset displays the three N_2 molecules solubilized in the ATMP matrix (red arrows). (e) For the 1 μs trajectory, accumulated time (t_{acc}) distribution of N_2 molecules that remain at a distance smaller than 4 Å from any atom of the surface during the trajectory. (f) Details of three solubilized N_2 molecules (the values of t_{max} are indicated).

Figure 2. High resolution XPS spectra for ATMP (a) as prepared and after treatment in a N_2 atmosphere at (b) 1 and (c) 6 bars. Curves in red correspond to experimental measure, while the dashed black line shows the envelope curve after sum the deconvoluted contributions centred at 400 eV (dark blue), 402 eV (orange) and 405 eV (pink). The solid black line corresponds to the background. (d) Variation of the weight percent contribution of the three N 1s components with the pressure of N_2 during the adsorption treatment.

Figure 3. (a) SEM micrograph of the p-HAp/ZC/ATMP catalyst. The distribution of the different components is displayed. (b) Assigned $^{1}H–^{15}N$ HSQC spectrum obtained

dissolving the catalyst and the reaction products from the synthesis of amino acids in deuterated water containing 100 mM HCl and 50 mM NaCl at 25 ºC. (c) TGA (left) and DGTA (right) curves of ATMP as purchased and after treatment with UV radiation at 95 ºC for 48 h.

Figure 4. ^{1}H NMR spectra of a sample obtained by dissolving the catalyst and products of reaction in an aqueous solution with 100 mM HCl and 50 mM NaCl at 25 ºC (black line) and the products and intermediates from decomposition of aminopolyphosphonates dissolved in the same solution (red lines). As shown, such decomposition compounds, which are aminomethylphosphonic acid (AMPA), 2-aminethylphosphonic acid (2-AEP), methylamine, *N*-phosphonomethyl-glycine (NMPG) and *N*-(methyl)glycine (SAR), do not correspond to the products of the reation.

Figure 5. (a) Schematic view of the reaction steps considered for the AM. The species adsorbed onto the substrate (*i.e.* either ZC or p-HAp) are displayed in red. (b) Free energy diagram for the reaction pathways of AM/ZC (blue) and AM/p-HAp (light brown) is displayed in the left, while the calculated reaction intermediates are shown in the right. The colour code used for the spheres is: red and light blue spheres for the oxygen and zirconium atoms of ZC (blue box); red, orange, light blue and white for oxygen, phosphor, calcium and hydrogen atoms of p-HAp (light brown box); and dark blue for nitrogen atoms of N_2 adsorbed on ZC and p-HAp surfaces.Theoretical calculations were performed considering that R^+ is H^+.

Figure 6. (a) Schematic view of the reaction steps considered for the DM. The species adsorbed onto the substrate (*i.e.* either ZC or p-HAp) are displayed in red. (b) Free energy diagram for the reaction pathways of AM/ZC (blue) and AM/p-HAp (light brown). The calculated reaction intermediates are shown as insets above the calculate

free energy profiles. The colour code used for the spheres is: red and light blue spheres for the oxygen and zirconium atoms of ZC (blue box); red, orange, light blue and white for oxygen, phosphor, calcium and hydrogen atoms of p-HAp (light brown box); and dark blue for nitrogen atoms of N_2 adsorbed on ZC and p-HAp surfaces. Theoretical calculations were performed considering that R^+ is H^+.

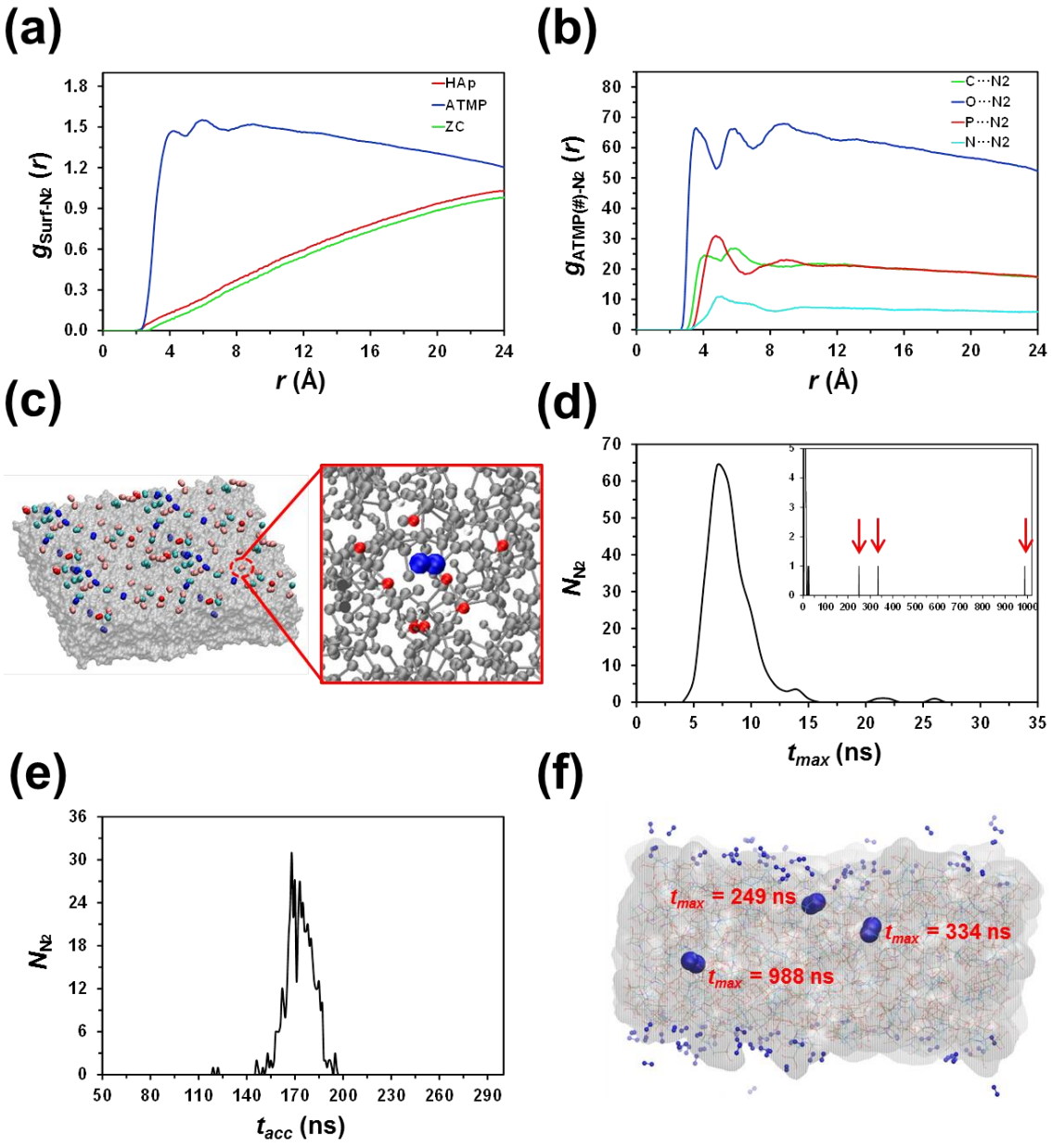
(a)
HAp
ATMP
ZC
$g_{Surf\text{-}N_2}(r)$
r (Å)
(b)
C···N2
O···N2
P···N2
N···N2
$g_{ATMP(\#)\text{-}N_2}(r)$
r (Å)
(c)
(d)
N_{N_2}
t_{max} (ns)
(e)
N_{N_2}
t_{acc} (ns)
(f)
t_{max} = 249 ns
t_{max} = 334 ns
t_{max} = 988 ns

Figure 1

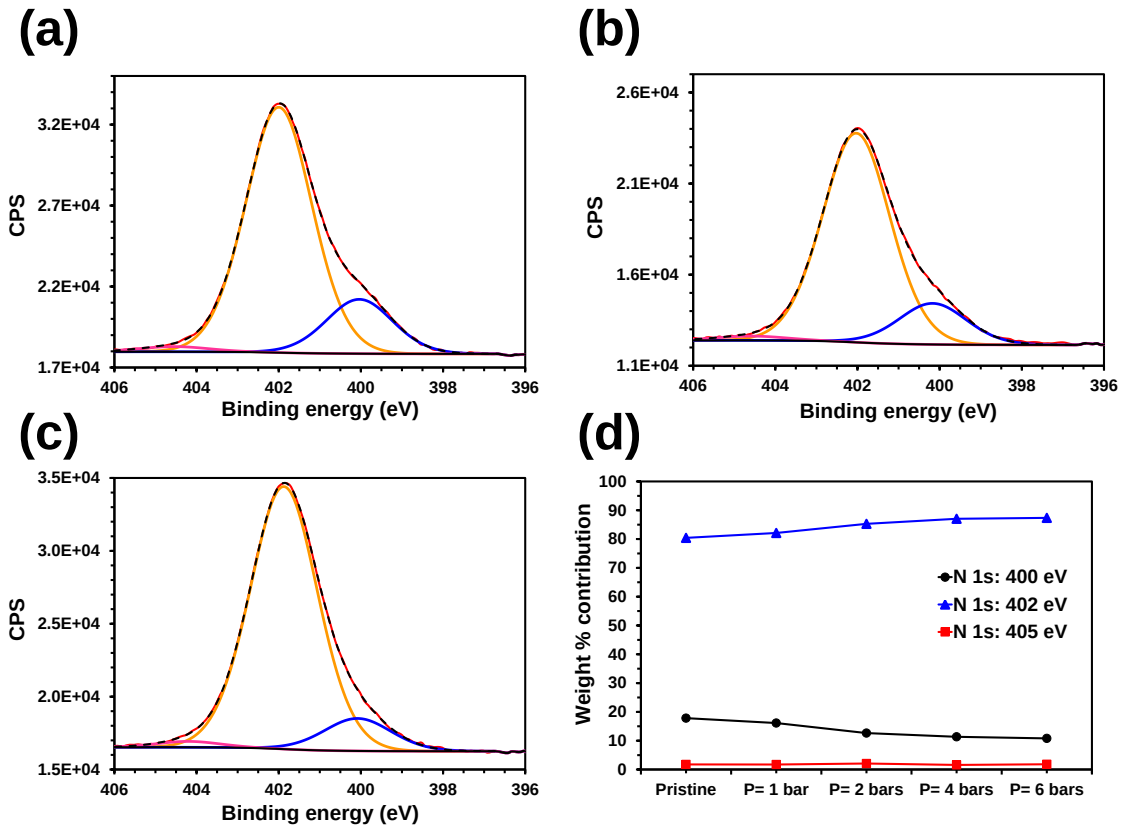
(a)
CPS
3.2E+04
2.7E+04
2.2E+04
1.7E+04
406
404
402
400
398
396
Binding energy (eV)
(b)
CPS
2.6E+04
2.1E+04
1.6E+04
1.1E+04
406
404
402
400
398
396
Binding energy (eV)
(c)
CPS
3.5E+04
3.0E+04
2.5E+04
2.0E+04
1.5E+04
406
404
402
400
398
396
Binding energy (eV)
(d)
Weight % contribution
100
90
80
70
60
50
40
30
20
10
0
N 1s: 400 eV
N 1s: 402 eV
N 1s: 405 eV
Pristine
P= 1 bar
P= 2 bars
P= 4 bars
P= 6 bars

Figure 2

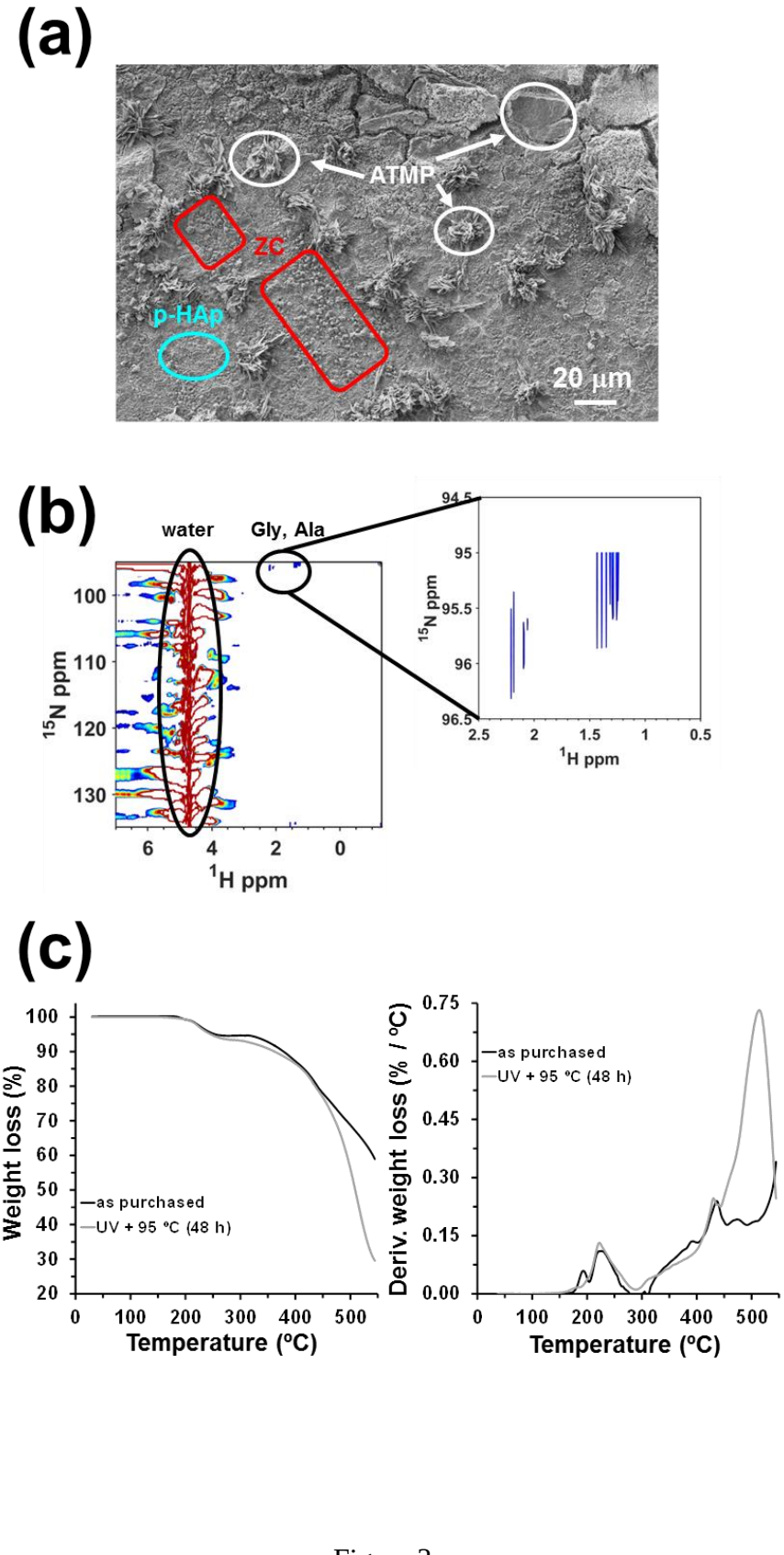
(a)
ATMP
ZC
p-HAp
20 μm
(b)
water
Gly, Ala
^{15}N ppm
^{1}H ppm
(c)
Weight loss (%)
Temperature (ºC)
as purchased
UV + 95 ºC (48 h)
Deriv. weight loss (% / ºC)

Figure 3

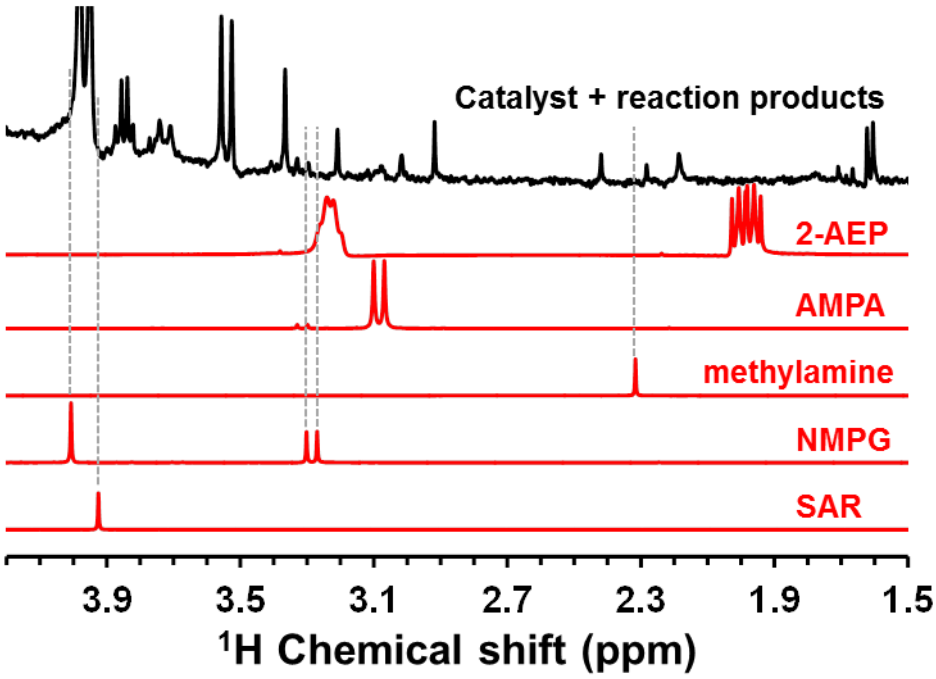
Catalyst + reaction products
2-AEP
AMPA
methylamine
NMPG
SAR
3.9
3.5
3.1
2.7
2.3
1.9
1.5
¹H Chemical shift (ppm)

Figure 4

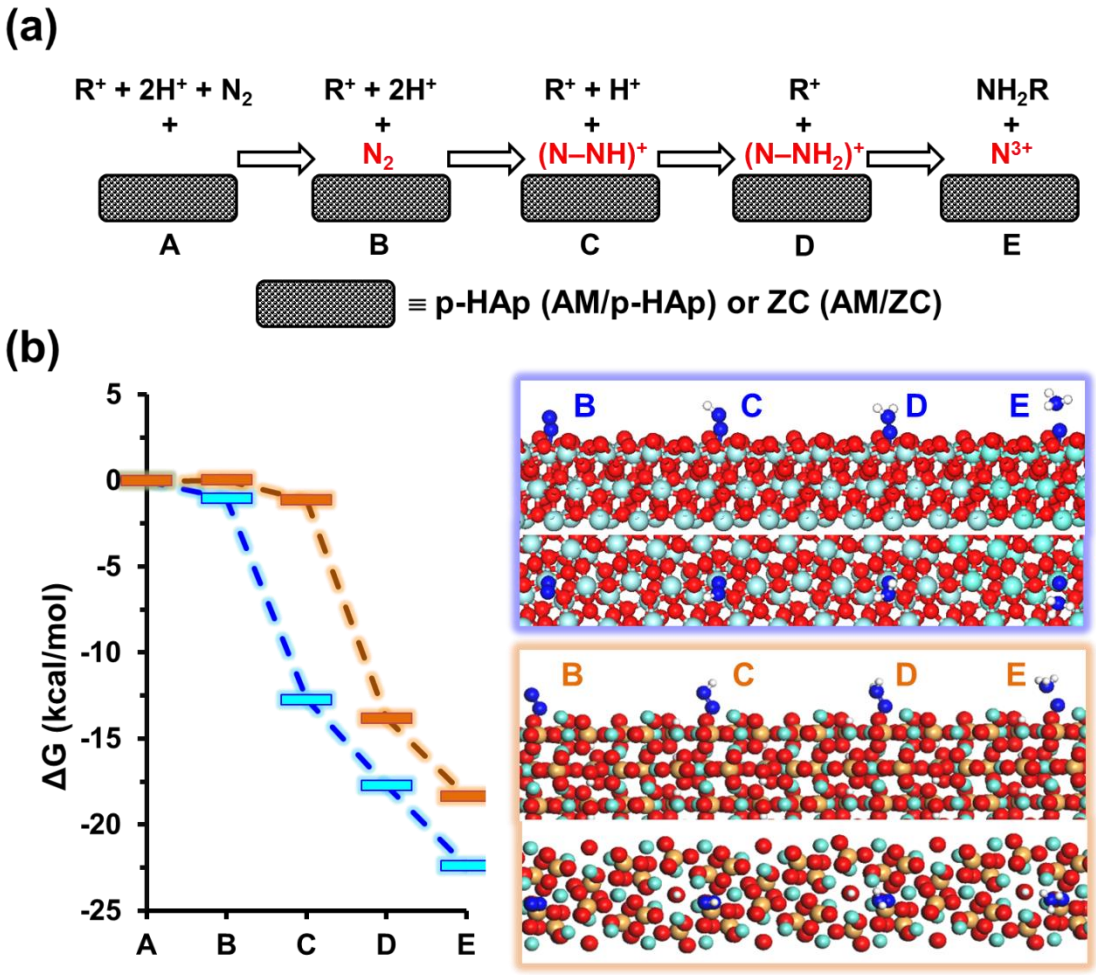
(a)
R+ + 2H+ + N2
+
A
R+ + 2H+
+
N2
B
R+ + H+
+
(N–NH)+
C
R+
+
(N–NH2)+
D
NH2R
+
N3+
E
≡ p-HAp (AM/p-HAp) or ZC (AM/ZC)
(b)
ΔG (kcal/mol)
5
0
-5
-10
-15
-20
-25
A
B
C
D
E
B
C
D
E
B
C
D
E

Figure 5

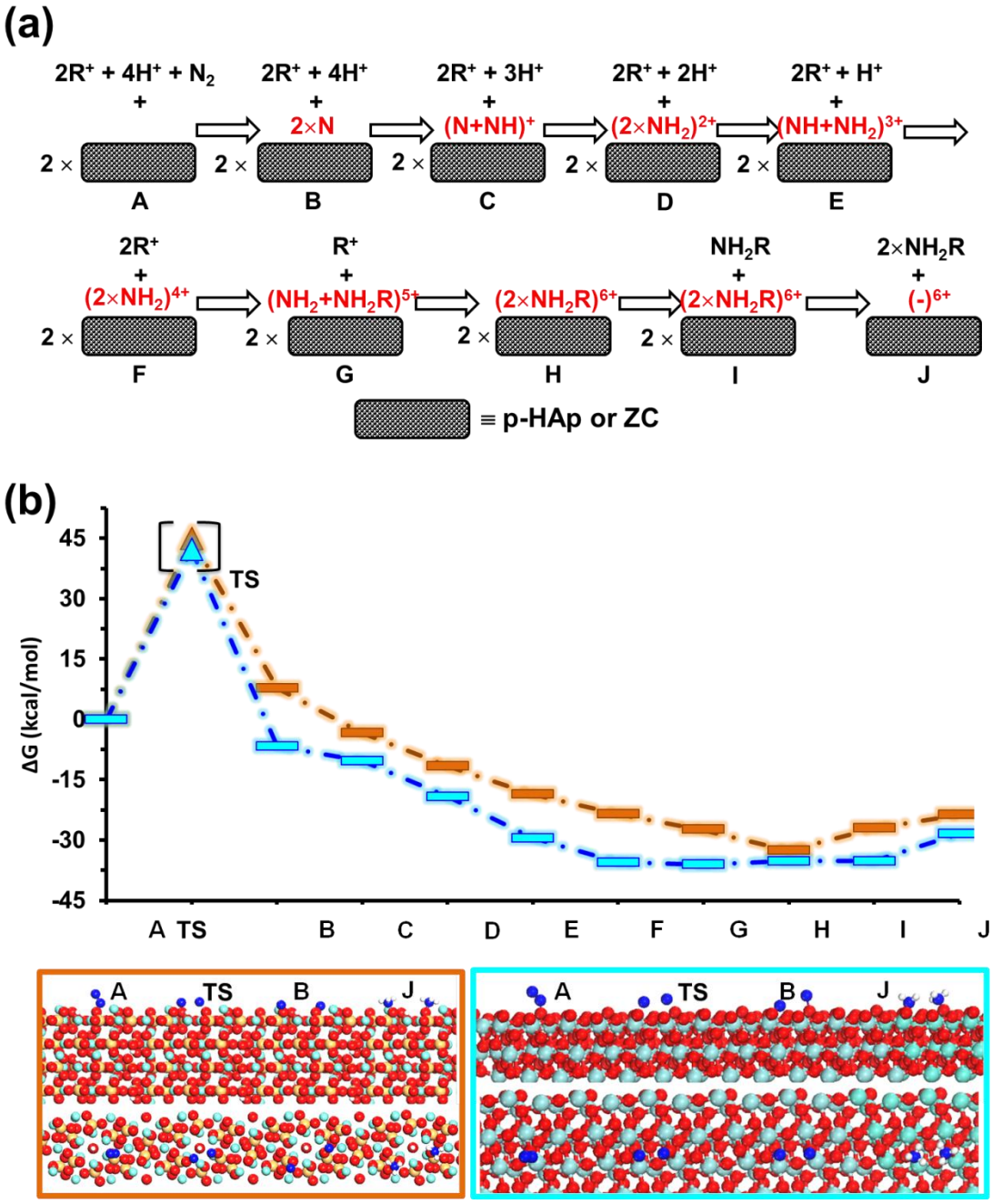
(a)
2R+ + 4H+ + N2
+
2 × A
2R+ + 4H+
+
2×N
2 × B
2R+ + 3H+
+
(N+NH)+
2 × C
2R+ + 2H+
+
(2×NH2)2+
2 × D
2R+ + H+
+
(NH+NH2)3+
2 × E
2R+
+
(2×NH2)4+
2 × F
R+
+
(NH2+NH2R)5+
2 × G
(2×NH2R)6+
2 × H
NH2R
+
(2×NH2R)6+
2 × I
2×NH2R
+
(-)6+
J
≡ p-HAp or ZC
(b)
ΔG (kcal/mol)
45
30
15
0
-15
-30
-45
TS
A TS B C D E F G H I J
A TS B J
A TS B J

Figure 6

TOC